COMMUNICATIONS IN SCIENCE AND TECHNOLOGY
Homepage: cst.kipmi.or.id

Understanding the regenerating capacity on photodegradation of methylene blue of titania supported mesoporous silica with the aid of gelatin-P123 as bitemplate

Maria Ulfa[a,*], Ika Uswatun Hasanah[a], Hasliza Bahruji[b]

[a]*Chemistry Education Study Program, Faculty of Teacher Training and Education, Universitas Sebelas Maret, Surakarta 57126, Indonesia*
[b]*Centre of Advanced Material and Energy Sciences, University Brunei Darussalam, BE 1410, Brunei Darussalam*

Article history:
Received: 14 June 2024 / Received in revised form: 28 October 2024 / Accepted: 29 November 2024

Abstract

Mesoporous silica (MS) was successfully synthesized via the sol-gel method using gelatin-P123 as a bi-template under hydrothermal reaction conditions at 100 ºC for 24 h, followed by calcination at 550 ºC for 5 h. The amount of TiO_2 in MS was adjusted to 1, 5, and 10% (w/w) and characterized using XRD, FTIR, SEM-EDX, N_2 adsorption-desorption, and UV-Vis. The crystallinity of the samples increased with higher TiO_2 content, as confirmed by XRD data. SEM analysis revealed that the morphology of MS and TiO_2/MS was cylindrical, with a particle size distribution of 0.4–0.6 µm. The surface area of MS was 500.8 m^2/g, which decreased to a range of 369.6–454.8 m^2/g after TiO_2 modification, while the pore diameter increased from 28.22 to 34.61 Å. The adsorption efficiency for methylene blue photodegradation reached a maximum value of 95%, demonstrating excellent catalytic performance. Thermal regeneration proved to be a promising strategy to recover the photocatalytic efficiency of TiO_2/MS for more than five cycles. Furthermore, thermal regeneration and the reuse of catalysts in wastewater treatment systems provide cost-effective solutions for pollutant removal.

Keywords: Titania; Mesoporous Silica (MS); gelatin; Pluronic P123; methylene blue; adsorption-photodegradation

1. Introduction

The rapid growth of the textile industry worldwide has resulted in a significant increase in dye waste, posing a severe threat to aquatic ecosystems due to the toxic nature of these pollutants, particularly aromatic hydrocarbons such as methylene blue ($C_{16}H_{18}ClN_3S$) [1,2]. Methylene blue is highly resistant to natural degradation, and its permissible concentration in water is limited to 5–10 mg/L [3,4]. This has driven researchers to explore innovative methods for methylene blue removal, beyond conventional physical processes such as coagulation and flocculation, which are often ineffective [5,6]. Advanced approaches, including Fenton processes [7], ozonation [8], photocatalysis [8], and adsorption [9-11] have shown promise, with photocatalysis standing out due to its ability to utilize light energy (UV light) to generate highly reactive hydroxyl radicals (OH^-) on the surface of semiconductor materials, thus accelerating organic pollutant degradation. The strong oxidative potential of hydroxyl radicals is crucial in enhancing dye removal efficiency [12,13].

Titanium dioxide (TiO_2) has emerged as a leading photocatalyst due to its chemical and biological inertness, non-toxic nature, low cost, and desirable photocatalytic properties. TiO_2, particularly in its anatase form, has a density of 3.9 g/cc, a bandgap energy of 3.2 eV, and oxygen vacancies that enhance its photocatalytic efficacy [14]. However, its inherent limitations, such as low surface area and high electron-hole recombination rates, restrict its full potential [15]. Recent research suggests that the impregnation of TiO_2 into porous materials can significantly improve its photocatalytic activity by increasing active sites and promoting efficient electron transfer [16]. Studies on TiO_2-zeolite composites have demonstrated limited color degradation, with only 60.4% removal achieved in 170 minutes, largely due to poor mesoporous accessibility and uneven catalytic site distribution [17–19].

Mesoporous silica has been identified as an ideal support material, with pore sizes ranging from 2 to 50 nm, which allows optimal access to methylene blue molecules (1.5 nm × 0.9 nm) [17–19]. This material's high surface area, large pore volume, and minimal microporosity make it ideal for facilitating molecular diffusion and maximizing catalyst exposure [17–19]. In previous research, mesoporous silica was synthesized using synthetic surfactants such as CTABr, P123, and F127 [19,20], but efforts are shifting toward more sustainable alternatives.

* Corresponding author. Tel.: +62-813-92923-2270
Email: mariaulfa@staff.uns.ac.id
https://doi.org/10.21924/cst.9.2.2024.1455

The use of natural surfactants, such as gelatin, in combination with synthetic surfactants, has yielded promising results in the synthesis of nanostructures like carbon microspheres and hematite with excellent porosity [21,22]. Gelatin, as a natural polymer rich in amino groups (-NH_2), has a strong affinity for silanol groups (Si-OH) in silica, promoting effective molecular rearrangement and nanostructure formation [23].

In this study, we propose the synthesis of mesoporous silica (MS) using a gelatin soft template in combination with P123, followed by the impregnation of TiO_2. This novel approach leverages the unique interaction between gelatin and silicate species to create an enhanced porous framework, facilitating improved photocatalytic performance in methylene blue removal via adsorption-photodegradation. The study further explores the regeneration capacity of the material, positioning it as a potentially sustainable and cost-effective solution for pollutant degradation.

2. Materials and Methods

Tetraethyl Orthosilicate (TEOS, pure analysis Sigma Aldrich) as silica source, Tetraethyl Ortho titanate (TEOT, $C_8H_{20}O_2Ti$, Sigma) as titania source, methylene blue (Mr 319,9 g/mol), HCl, Gelatin as green template, n-hexane as solvent, Pluronic P123 as co-template. All chemicals are analytical grade.

2.1. Synthesis of mesoporous silica (MS)

MS synthesis was initiated by mixing P123 and Gelatin into 37% HCl which had been diluted in water. The mixture was stirred at a temperature of 40°C with a rotational speed of 500 rpm for 3 h. TEOS was then added to the mixture. Then, the stirring process was continued with the same temperature and speed for 24 h. The ratio of Gelatin: P123: H_2O: HCl: TEOS was 0.04: 4: 19.5: 127: 9.24 (w/w/v/w). Afterward, the sample was put in a hydrothermal autoclave. Next, it was heated using an oven at 90°C for 24. The resulting solid was dried and calcined in a furnace at 550°C for 5 h producing a white powder. The powder was then activated with 50 mL of 0.1 M HCl for 24 h followed by filtering, washing, and drying for 24 h at 100°C producing the final sample. The final sample was named NMCS.

Table 1. The notation of the synthesized samples

Sample	%w/w TiO_2/MS	V TEOT (ml)
MS	0.00:1	0.000
1- TiO_2/MS	0.01:1	0.023
5- TiO_2/MS	0.05:1	0.122
10-TiO_2/MS	0.10:1	0.244

2.2. Modification of MS by TiO_2 impregnation

MS was modified by dissolving 0.024 mL of Tetraethyl Orth titanate (TEOT) in 20 mL of n-hexane, then added to 0.99 grams of MS powder. The mixture was stirred at 45°C for 16 h followed by drying at 160°C for 2 h and washing with hexane. The solid was re-dried at 80°C for 45 min followed by calcination in a furnace at 550 °C for 5 h forming TiO_2/MS. The weight of TiO_2 was varied to produce the % weight of Titania in MS of 1, 5, and 10 labeled as in Table 1.

2.3 Characterization of the catalyst

Nitrogen (N_2) adsorption-desorption was performed on a Quantachrome Autosorb Automated Gas Sorption System, with an outgas temperature of 200°C and a bath temperature of 77 K. Analysis of the N_2 adsorption data was performed at Autosorb 1® for windows 1.2 provided by Quantachrome Co. The surface area was calculated using a multipoint BET model using the P/P_0, ranging from 0.05 to 0.2. The PSD was computed using a BJH model, and the total pore size was estimated in terms of the maximum P/P0 point. The crystalline phase of the samples was investigated via Philips X'pert X-ray diffraction (XRD) instrument with Cu-Kα radiation, a step size of 0.04°, and a counting time of 10 s. The data were recorded in the 2θ range of 5-80°.

$$Cristalinity = \frac{cristalline\ peak\ area}{cristalline\ and\ amorphous\ peak\ areas}\ x\ 100\% \quad (1)$$

The crystallinity was measured using the XRD peaks widening as Eq. 1. Additionally, to identify the sample phase, the XRD data were used to calculate the crystal size of the MS using the Debye Scherrer formula as Eq. 2.

$$D = \frac{0.9\lambda}{B cos\theta} \quad (2)$$

In which, D is the crystal size in Å, λ is the wavelength of X-Ray source (λCu = 1.54056 Å), B is the half-peak width in radians, and θ is the diffraction angles. XRD results also show full width at half maximum (FWHM) to determine the B value (rad). Quantitative analysis results were obtained from sample calculations using X-Ray Diffraction data.

The morphology and elements of the samples were observed via Scanning Electron Microscopy combined with Electron Dispersive Spectrometer (SEM-EDX) from ZEIS EVO MA 10 by coating the samples using Pd/Au. The SEM data were analyzed using Origin 7.0 software to obtain the histogram of the particle size distribution. The functional groups' analysis was conducted in the range of 400-4000 cm^{-1} by Fourier transform infrared spectroscopy (FTIR) from Shimadzu Spectrometer 2800. UV–vis spectral data were taken in Cary 500 Scan UV–vis–NIR spectrophotometer provided with an integrating diffuse reflectance accessory. The spectra recorded in the range 200–500 nm in terms of F(R), the Kubelka–Munk function, were used to calculate the bandgap of the TiO_2 materials.

2.4 TiO_2/MS Activity in adsorption-photodegradation of methylene blue (MB)

The application began by forming an initial solution of MB with a concentration of 5 ppm as much as 200 mL. The photocatalytic process started with dark adsorption by introducing 5 mg photocatalyst in a reactor containing 10 ml of 5 ppm MB solution. It was then stirred for 30 min followed by a photocatalytic reaction using UV lamp irradiation with various irradiation times of 5, 10, 15, 20, 30, 40, 50, 60, 70, 80, 90, and 120 min. The absorbance of each irradiated MB solution was then measured using a UV-Vis spectrophotometer

with a wavelength of 665 nm. The percentage of MB degradation was estimated using Eq. 3 which the concentration of the solution could be determined from the absorbance curve of the sample.

$$(\%D) = \frac{C_o - C_t}{C_o} \text{ x } 100\% \quad (3)$$

In which, C_o is the initial MB concentration (before irradiation), C_t is the MB concentration after *t* min irradiation, and $\%D$ is the degradation efficiency or degradation percentage. Kinetic models were used to analyze the kinetic data relating to the photocatalytic degradation of MB on TiO_2/MS, as presented in Table 2.

Table 2. Kinetic Model to analyze photocatalytic degradation of MB

Model	Equation Formula
Pseudo zero orders	$C\_o - C\_t = kt$
Pseudo first order	$〖Ln\ (C〗\ \_o - C\_t) = -kt$
Pseudo second order	$1/C\_o\ - 1/C\_t\ = kt$

3. Results and Discussion

3.1. Catalyst preparation

Surface area analysis using the BET method was performed to determine the surface area, pore volume, and pore diameter of the samples, as shown in Fig. 1. The adsorption-desorption isotherms of all samples exhibited Type IV isotherms, characteristic of mesoporous materials. The samples also showed hysteresis with an H-1 type form, indicating a narrow pore size distribution. After titania impregnation, the hysteresis loop at the relative pressure (P/P0) in the range of 0.4–0.9 shifted, indicating the presence of TiO_2 loading in the MS. The bimodal pore size distribution showed peaks in the range of 18.22–34.61 Å. In general, higher TiO_2 loading in MS silica results in larger pore sizes due to the inclusion of organic and inorganic components of TEOT as Ti precursors, which causes the swelling of MS pores due to the deposition of Ti elements in the inner pores.

3.2. Regeneration

Regeneration testing and catalyst reuse were carried out by separating the catalyst from the methylene blue filtrate of the first photocatalytic cycle. The catalyst was then suspended in 200 cm³ of ultrapure water and heated to a temperature of 200–600°C for 3 hours. After thermal processing, the catalyst was separated by filtration, washed with water, and dried in a vacuum overnight. The dried sample was then used as the catalyst in the next catalytic cycle.

Table 3 presents the textural properties of all samples. The surface area decreases as the TiO_2 content increases in MS due to pore-blocking by Ti and C, which will be further confirmed by EDX analysis. The pore volumes do not exhibit a significant change, remaining in the range of 0.62 to 0.70 cc/g, although TiO_2 loading in MS continues to reduce the total pore volume. Silica, with the largest pore volume, is MS with a value of 0.7065 cc/g. However, based on the results, the presence of TiO_2 loading in MS expands the mesoporous volume. These results indicate that some TiO_2 particles are dispersed into the MS pores, which causes the total pore volume and BET surface area to decrease.

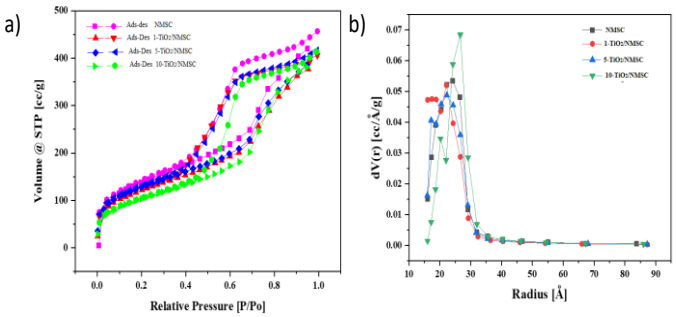

Fig. 1. (a) Adsorption-Desorption N_2 and (b) Pore size distribution of MS before and after titania impregnation

Table 3. Physiochemical properties of samples

Sample	Particle size (μm) [a]	Elemental analysis (%W) [b]			Porosity analysis [c]		
		O	Si	Ti	S (m^2/g)	V (cc/g)	R (A)
MS	0.52	54.12	45.88	0.00	500.80	0.719	28.22
TiO_2/MS 1%	0.39	63.28	35.10	1.62	435.45	0.669	28.80
TiO_2/MS 5%	0.43	68.76	28.10	3.14	454.40	0.654	28.21
TiO_2/MS 10%	0.37	64.88	30.87	4.30	369.00	0.635	34.60

[a] Particle size from SEM
[b] %W from EDX
[c] Porosity from Nitrogen adsorption-desorption (S=Surface area from BET, V=pore volume, R=pore radius from Desorption Branch in BJH analysis)

The elemental analysis results obtained using Energy Dispersive X-ray (EDX) confirmed that all samples contained silicon (Si) and oxygen (O), indicating that the mesoporous silica (MS) samples, both before and after titania impregnation, are silica-based materials. The 1%, 5%, and 10%-TiO_2/MS samples showed Ti content ranging from 1% to 4%, confirming the successful impregnation of TiO_2 into the MS structure via the hard templating method. The Ti content increased proportionally with the mass percentage of TiO_2 deposited on the MS. However, the Ti content in the 1%, 5%, and 10%-TiO_2/MS samples (ranging from 1.6% to 4.3%) was slightly lower than the expected TiO_2 weight (1%-10%). This discrepancy is likely due to the impregnation process, which involved a single infiltration step, resulting in Ti being trapped within the inner silica walls while some TiO_2 dispersed onto the outer surface. It is possible that Ti ions are preferentially deposited on the outer silica walls, increasing the wall thickness. Another factor is the competitive interaction between Ti and Si (from the tetraethyl orthotitanate, TEOT, precursor) during the impregnation. As TEOT integrates into the MS pores, organic groups with sizes larger than Ti ions may cause partial pore-blocking at the pore mouths, limiting the penetration of Ti into the inner pores. Consequently, Ti predominantly interacts with the outer surface of the MS. Additionally, the one-step impregnation process could result in some Ti that electrostatically interacts with the MS surface being washed away during the hexane washing process, leading to a lower measured Ti content compared to the amount initially impregnated.

Fig. 2 illustrates the dispersion of titania following impregnation. The silicon (Si) content decreases from 45% to 28-35% by weight before and after impregnation, attributed to the incorporation of titanium (Ti) components. The oxygen content in the mesoporous silica (MS) before impregnation (54.12%) is primarily due to the Si-O interactions formed during the soft templating process with P123. As shown in Table 4, the total Si content after titania impregnation decreases from 45% to 28-35%, a trend that is likely due to the formation of Ti-O and Si-O bonds, which increase the oxygen content in the structure. The impregnation of TiO_2 into the MS is analogous to the nano-casting process employed in hard-templated ordered mesoporous materials, where precursor materials are partially deposited into both the inner and outer pores of the hard template. Tetraethyl orthotitanate (TEOT) interacts with the silica walls at both the inner and outer surfaces, and upon calcination, it decomposes to form Ti-O and Si-O linkages. This interaction results in a reduction of Si content but an increase in oxygen content due to the presence of titanium. These changes are further corroborated by the X-ray diffraction (XRD) results

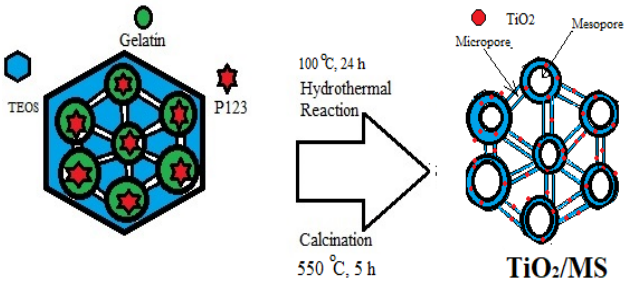

Fig. 2. Schematic soft templating route by P123 and gelatin stabilizing silica in aqueous phase to produce MS with TiO_2 impregnation

Table 4. Crystallinity and particle diameter of MS before and after TiO_2 impregnation

Sample	Crystallinity (%)	*D* (nm)
MS	23.27%	5.68
1-TiO_2/MS	26.16%	7.96
5-TiO_2/MS	31.60%	10.87
10-TiO_2/MS	43.56%	27.91

D= Crystalite size from Debye Scherrer Equation

Fig. 3 presents the XRD patterns of all samples before and after impregnation. The MS sample exhibits an amorphous peak at 25.2135˚, characteristic of amorphous SiO_2. Upon impregnation with a high TiO_2 loading, distinct Ti peaks are observed at 37.9303˚, 48.0165˚, 54.1502˚, and 62.9145˚, which correspond to the anatase phase, as identified in the JCPDS database. For samples with low TiO_2 loading, the Ti peaks are less pronounced due to the lower Ti content within the MS. Notably, after titania impregnation, MS retains its structural integrity with minimal damage, indicating high stability during the metal oxide impregnation process. The crystallinity and crystal size of the samples increase with higher TiO_2 content, with the dispersion of TiO_2 within the MS being uniform. This uniform dispersion contributes to a twofold increase in crystallinity compared to the pre-impregnation state, likely due to the crystallization of titania during high-temperature treatment. Additionally, the crystal size expands post-impregnation, suggesting that the incorporation of TiO_2 into MS induces an increase in crystal size, which is consistent with the results from pore size distribution observed through N_2 adsorption-desorption. However, the silica framework's arrangement diminishes, as indicated by the reduced intensity of certain XRD peaks. This alteration can be attributed to the expansion and contraction of silica pores during Ti precursor infiltration and the decomposition of organic functional groups.

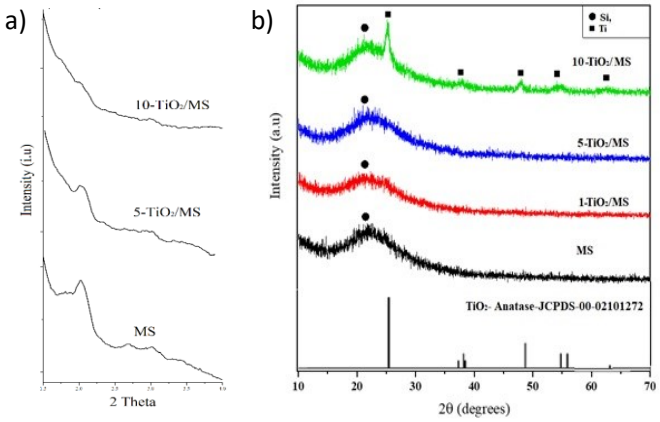

Fig. 3. Diffractogram (a) low and (b) wide angle of XRD

Fig. 4 presents the FTIR spectra of all samples before and after impregnation. All samples exhibit a broad absorption band in the hydroxyl (-OH) region, centered around 3400 cm^{-1}, corresponding to the stretching vibration of the Si-OH functional group. Absorption peaks observed at wavenumbers approximately 1070 cm^{-1} and 800 cm^{-1} are characteristic of the Si-O-Si bond stretching vibrations. Additionally, a peak at 1650 cm^{-1} is indicative of Si-OH stretching, confirming the presence of silica-hydroxyl functional groups in all samples. After the impregnation process, the intensity of the Ti-OH bending vibration at 475 cm^{-1} increases. The areas of each absorption band in the FTIR spectra demonstrate that the impregnation process was successfully carried out without causing significant alterations to the structure or functional groups of the MS. This conclusion, indicating no substantial structural changes in MS before and after titania impregnation, is consistent with the findings from the SEM analysis.

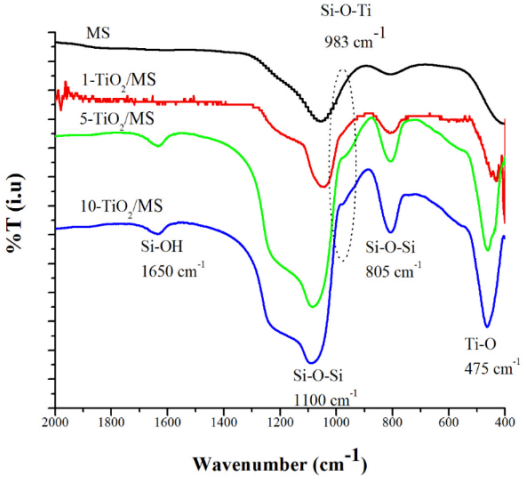

Fig. 4. IR spectra of MSs before and after titania impregnation

Fig. 5 illustrates the morphological characteristics of all samples, revealing rod-shaped particles with pronounced agglomeration in certain regions. This suggests that the TiO_2 impregnation process does not induce significant alterations to the morphology of the MS particles. The histogram analysis indicates that the average agglomeration size of the particles ranges between 0.3 and 0.5 µm. Notably, the most substantial increase in agglomeration size is observed in the MS sample with 5% TiO_2 loading, likely due to the attractive interactions between the TEOT precursor and the MS matrix. Simultaneously, the particle size decreases as the TiO_2 content increases, which can be attributed to an enhanced atomic packing factor arising from the deposition of TiO_2 within the internal pores. This effect is further exacerbated by the compressive forces induced during the double calcination process, which follows impregnation.

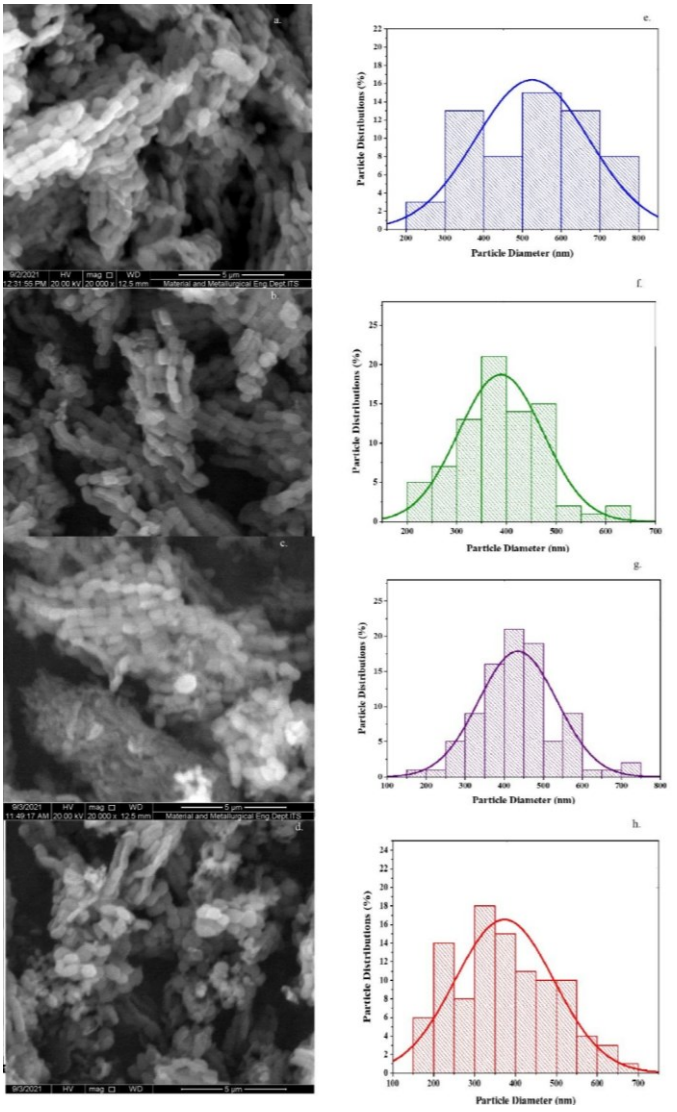

Fig. 5. SEM images and particle size distribution of (a,e) MS (b,f) 1-TiO_2/MS (c,g) 5-TiO_2/MS (d,h) 10-TiO_2/MS

Fig. 6 presents the 2D morphology of the MS samples, both before and after titania impregnation, as observed through TEM. The samples exhibit a hexagonal arrangement, which remains uniform before and after impregnation. After titania impregnation, the hexagonal arrangement of the MS features a single pore surrounded by six smaller pores, with an inhomogeneous distribution of TiO_2 across the MS silica surface. The pore size distribution, as shown in Fig. 7, shifts from a range of 3.0-6.5 nm to 3.5-8.0 nm, with the maximum pore size decreasing from 5.5 nm to 4.0 nm. Despite these changes, no significant structural alterations are observed in the overall morphology of the MS after impregnation.

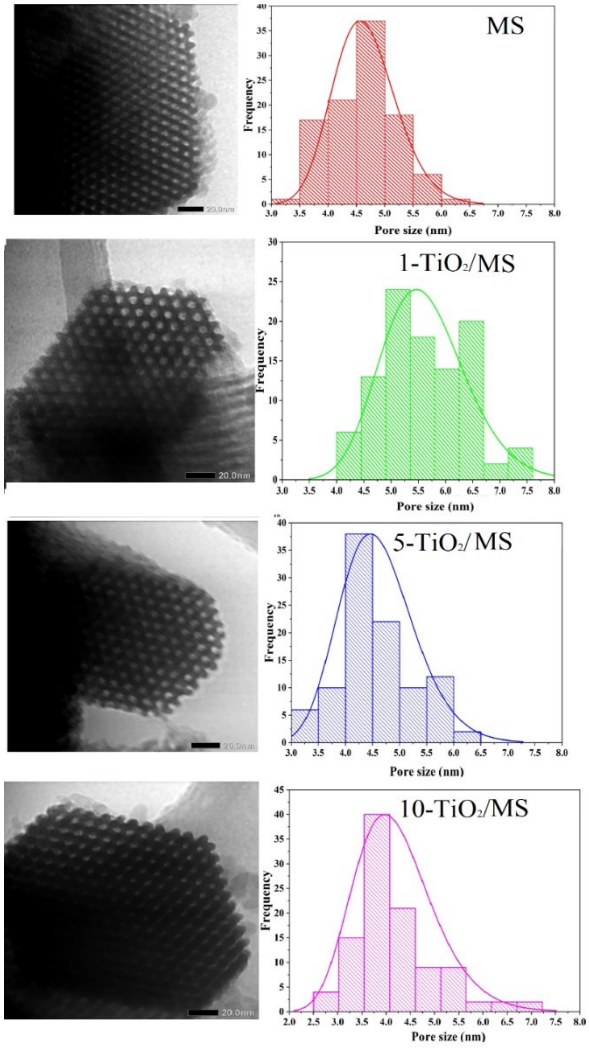

Fig. 6. TEM lattice image of the TiO_2/MS samples calcined at different titania concentration

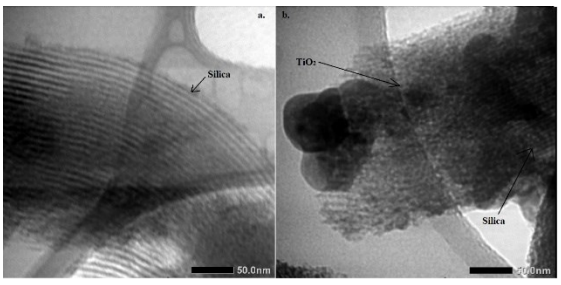

Fig. 7. The transmission electron microscope silica MS before (a) and after titania impregnation (b)

The Raman spectra of MS shown in Fig. 8 displayed sharp peaks at 1060 and 1250 cm^{-1} indicating S-O-Si stretching. After titania impregnation, sharp peaks appeared at both the 1 and 10% TiO_2 concentrations, namely at the peaks of 399, 520 and 650 cm^{-1} correspond with an anatase crystal structure which

implied with successful titania impregnation process into mesoporous silica. This result is in line with the research [21,22].

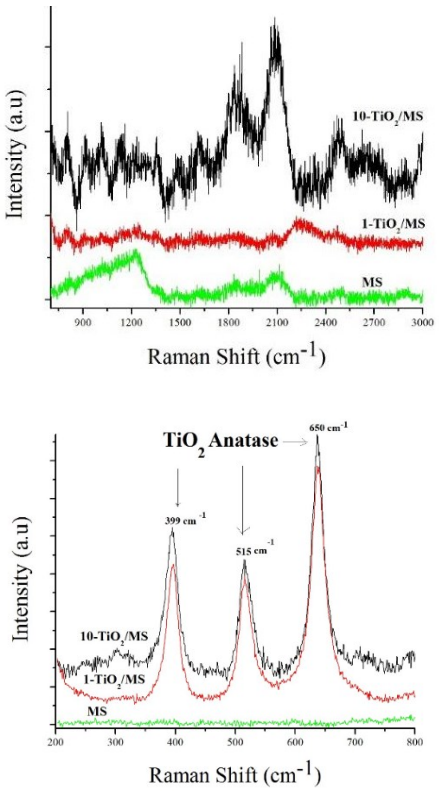

Fig. 8. Raman scattering of the waveguides for mesoporous silica before and after titania impregnation

3.3. Adsorption-photodegradation activity of MB

Fig. 9 illustrates the dual system process for methylene blue (MB) removal via dark adsorption-photodegradation using MS samples before and after impregnation. The degradation of MB improves with increasing UV irradiation time. Notable degradation increases occur between 5 and 40 minutes of irradiation, after which the degradation reaches equilibrium between 40 and 90 minutes. The results from the dual removal system demonstrate that all post-impregnation samples achieve an average efficiency of 77-95%. The dark adsorption process alone can degrade MB by approximately 30-65%, owing to the high surface area of the MS material. The highest degradation yield of 95% is achieved by 10-TiO_2/MS, attributed to its large surface area and Ti content, which acts as an active catalytic center. A comparison of surface area and degradation percentage between 1-TiO_2/MS and 10-TiO_2/MS further supports this: the surface areas of 1-TiO_2/MS and 10-TiO_2/MS are 434 m²/g and 360 m²/g, respectively, resulting in 87% and 95% degradation. Despite having a lower surface area, 10-TiO_2/MS achieves 95% degradation due to its higher Ti content as a catalytic center. In contrast, 1-TiO_2/MS degrades MB by only 45%, despite its higher surface area, due to the lack of sufficient catalytic centers. Overall, all samples exhibit excellent degradation performance.

The photocatalytic activity of MS and 1-TiO_2/MS is displayed in Fig. 10 presents that the absorbance curve declines with increasing contact time with MB and has an efficient percentage of 45.1 and 95.2 %, respectively. The results are similar to previous studies on other supporting materials that achieved an efficiency of pure titania oxide and impregnated into SiO_2 in the range of 70 – 90% [23]. The enhanced oxidation rate due to the presence of titania active sites in MS is confirmed by the spectrophotometric analysis of the treated solution, as shown in Fig. 11. The reduction in MB concentration exceeds the decrease in absorbance at the maximum wavelength, with a hypochromic shift upon contact with the material, indicating changes in the chemical structure of MB. The initial rate of MB concentration reduction highlights the role of titania in accelerating the degradation process, achieving a twofold increase in degradation rate compared to MS alone. The faster MB degradation with increasing Ti content is attributed to the more rapid formation of radicals, driven by the increased number of holes during the reaction mechanism. Overall, TiO_2/MS achieves approximately 95% MB degradation within the first 60 minutes, whereas MS requires 90 minutes to degrade 50% of MB under the photooxidation mechanism. A similar degradation percentage is observed after about 120 minutes through the photocatalytic mechanism. This enhanced performance is likely due to the bandgap energy of Ti-containing materials, coupled with the larger specific surface area and pore volume in TiO_2/MS materials.

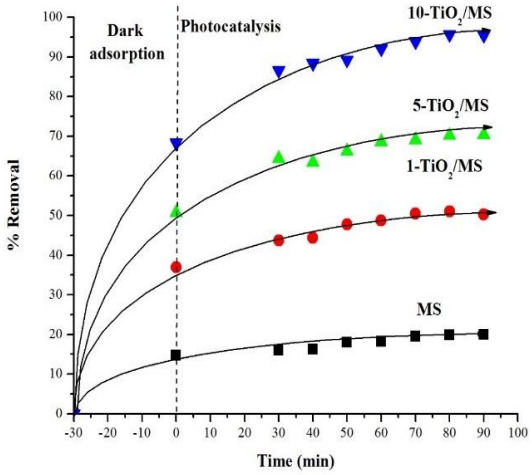

Fig. 9. Simultaneous adsorption-photodegradation of MB with TiO_2/MS

Table 5. MB degradation kinetics model using MS after titania impregnation

Sample	Photodegradation activity					
	Pseudo Zero-Order		Pseudo First-Order		Pseudo Second - Order	
	R^2	k	R^2	k	R^2	k
MS	0.775	10^{-3}	0.953	$3.\ 10^{-3}$	0.948	$3.\ 10^{-5}$
1-TiO_2/MS	0.756	$3.\ 10^{-3}$	0.909	$3.\ 10^{-3}$	0.925	$8.\ 10^{-5}$
5-TiO_2/MS	0.737	$5.\ 10^{-3}$	0.832	$3.\ 10^{-3}$	0.867	$3.\ 10^{-6}$
10-TiO_2/MS	0.739	$6.\ 10^{-3}$	0.827	$3.\ 10^{-3}$	0.871	$3.\ 10^{-6}$

Fig. 11 shows the UV–vis adsorption spectra of calcined TiO_2/MS and nanosized titania. It is observed that there is a blue shift of the ultraviolet light adsorption edge of TiO_2/MS compared with the nanosized anatase pure TiO_2. The blue shift is introduced by the quantum effect of the semiconductor compound [24,25]. TiO_2 has a bandgap of 3.27 eV, making it the semiconductor with the largest bandgap among all the

samples. However, as the TiO_2 impregnation dose increases, a decrease in the bandgap is observed, likely due to the role of TiO_2 as a semiconductor. A blue shift is observed in the samples after impregnation, which is attributed to the well-known quantum size effect for semiconductors, as the particle size decreases, consistent with the SEM results. The blue shift in the adsorption edge indicates an increase in the forbidden band energy (Fig. 12). According to quantum theory, the larger the particle size of the semiconductor compound, the lower the forbidden band energy. Therefore, the blue shift of the adsorption edge in the UV–vis scattering pattern suggests a decrease in the TiO_2 particle size. Additionally, the UV-Vis scattering pattern provides evidence of the coordination of Ti^{4+} in the TiO_2.

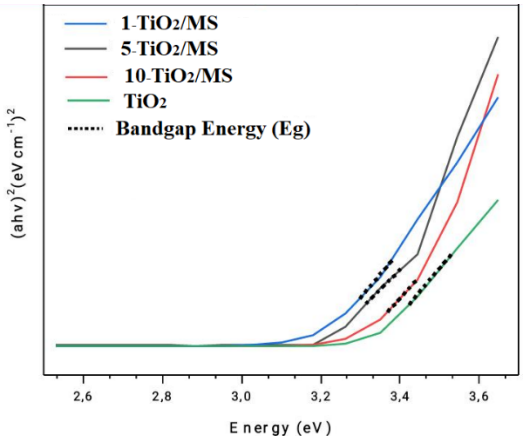

Fig. 10. UV-Vis spectra evolution of MB degradation using TiO2/MS photocatalyst

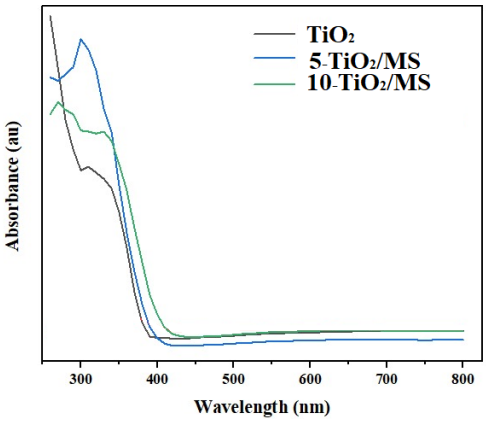

Fig. 11. UV-Vis Spectra of UV–vis adsorption spectra of calcined TiO_2/MS and nanosized titania

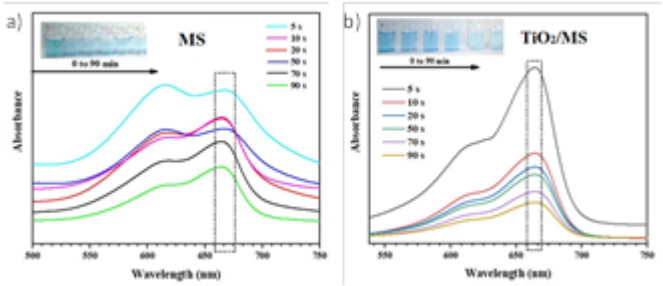

Fig. 12. UV-Vis Spectra of MB solution by Adsorption-Photodegradation using MS (a) before and (b) after titania impregnation

During photodegradation, hydroxyl (OH) radicals are generated, which degrade methylene blue (MB) molecules, resulting in overall enhanced efficiency. The results indicate that the 5-TiO_2/MS photocatalyst exhibits the lowest degradation performance among all samples. This is consistent with the BET test results for the 5-TiO_2/MS photocatalyst, where the prominent role of micropores prevents some MB molecules from entering the pores, thus limiting degradation to the mesopores. This process continues under UV light, with the catalytic center containing approximately 2% Ti content. The degradation kinetics, as shown in Table 6, suggest that the sample after impregnation follows a pseudo-second-order model with an R^2 value of 0.97 for the 5-TiO_2/MS, indicating that the degradation process under UV light fits the model for the formation of multilayer molecules during photodegradation. The kinetics also reveal that the dark adsorption-photodegradation treatment alters the linearity of the pseudo-second-order model, with an R^2 value of 0.93 for the 5-TiO_2/MS. In comparison, the linearity is lower for other samples. This phenomenon is likely due to the role of absorption at the onset of degradation, which affects the correlation between MB concentration and the total degradation percentage. Overall, the degradation of MB by TiO_2/MS functions effectively due to the combined action of dark adsorption and photocatalysis.

Table 6. Band gap of MS before and after TiO_2 impregnation

Sampel	Energy (eV)
1-TiO_2/MS	3,10
5-TiO_2/MS	3,14
10-TiO_2/MS	3,22
TiO_2	3,27

3.4. TiO_2 Loading and photocatalytic mechanism

The enhancement in photocatalytic performance due to TiO_2 loading is closely linked to the structural and surface properties of the TiO_2/MS composite. As TiO_2 content increases, surface area, pore volume, and pore size (radius) change, which are crucial for improving photocatalytic activity. The surface area slightly decreases from 500.8 m^2/g for pure MS to 369.0 m^2/g for TiO_2/MS 10%, but the average pore radius increases to 34.6 Å, suggesting that larger pores are formed, allowing more methylene blue (MB) molecules to access the catalyst surface, thus enhancing mass transfer during the degradation process. Elemental analysis confirms an increase in Ti content, directly correlating with more active sites for the photocatalytic process. This is reflected in the increase in MB degradation efficiency from 45.1% for pure MS to 95.2% for TiO_2/MS, demonstrating that TiO_2 accelerates the degradation process. The higher TiO_2 content also reduces the bandgap energy from 3.27 eV for TiO_2 to 3.10 eV for TiO_2/MS, facilitating more efficient utilization of UV light and improving photocatalytic activity. The combination of larger pores, increased surface area, enhanced TiO_2-silica interactions, and reduced bandgap energy significantly boosts the formation of hydroxyl radicals, enhancing the photocatalytic degradation of methylene blue.

3.4 Regeneration

Thermal regeneration of the catalyst was performed using

10%/TiO_2/MS by treating the methylene blue loaded TiO_2/MS at 200, 400 and 600 °C for 180 min under the oxygen atmosphere (Fig 13).

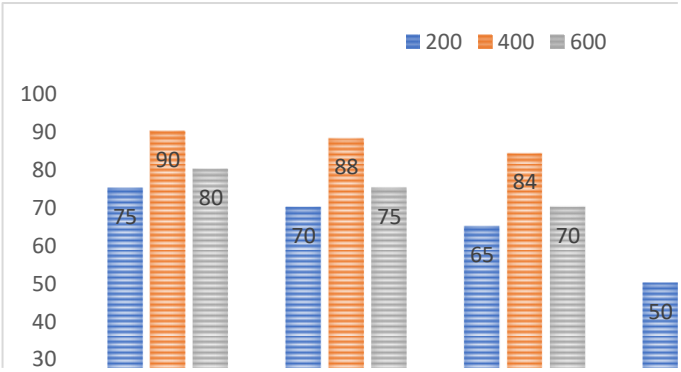

Fig. 13. Thermal regeneration effect on photocatalytic performance In general, the removal performance

The percentage of removal (%) by the regenerated catalyst was lower compared to the freshly prepared material, which can be attributed to the decrease in active binding sites caused by methylene blue coverage. As shown in Fig. 12, a temperature of 200°C in the 1st to 5th regeneration cycles exhibited the lowest efficiency, compared to temperatures of 400°C and 800°C. This is expected, as the low temperature does not facilitate the complete decomposition of methylene blue bound to the catalyst surface. Fig. 12 indicates that 400°C is the optimal temperature for TiO_2/MS regeneration, as it yields the highest total regeneration efficiency compared to 600°C and 200°C. Although 600°C demonstrates higher regeneration performance than 200°C, the increased energy requirements make it less favorable.

To assess the variations in catalyst performance during solvent-based regeneration, the effects of solvents such as methanol and ethanol were examined. As shown in Fig. 14, a similar trend was observed across cycles 1 through 5, with methanol performing marginally better than ethanol. The regeneration efficiency for both solvents peaked in cycles 1-2 but declined sharply in cycles 3-5. This decline is attributed to the increasing accumulation of methylene blue within the inner framework during cycles 1-2, which hinders its effective dissolution in subsequent cycles, thus reducing the regeneration capacity in cycles 3-5.

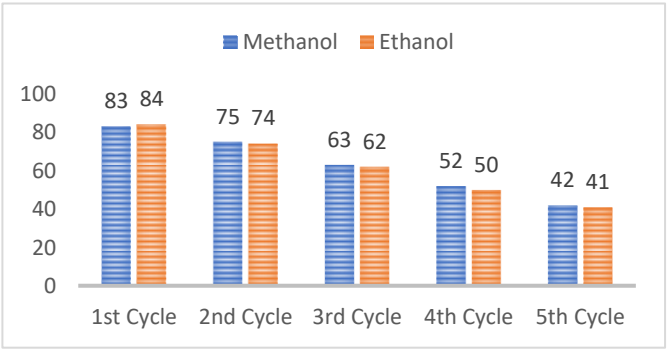

Fig. 14. Solvent Regeneration effect on photocatalytic performance (300 ml solvent on room temperature during 3 h)

The methylene blue removal efficiency after five regeneration cycles was approximately 42% (Fig. 15). Removal studies reveal that mild thermal regeneration at 200 °C for 1 hour is more effective than the solvent method using ethanol for 12 hours. This is likely due to the fact that the lower regeneration temperature facilitates the displacement of methylene blue from the catalyst framework, making it easier to wash away. This approach presents a promising strategy for effective catalyst recovery from waste solutions.

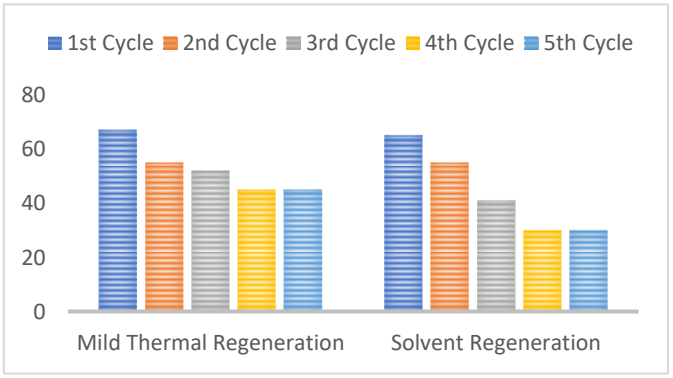

Fig. 15. Effect mild thermal regeneration(200 °C, 1 h) and Ethanol regeneration 12 h

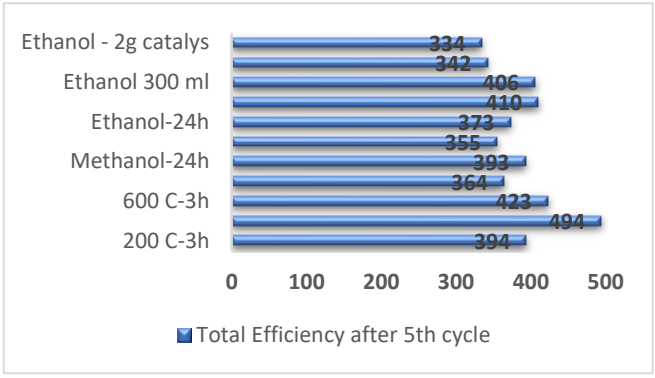

Fig. 16. Effect different condition regeneration on economical catalyst value

The catalyst regeneration process, evaluated over five distinct stages, demonstrated a remarkable overall efficiency of 494% (Fig. 16) under thermal regeneration conditions sustained for three hours. While solvent-based regeneration using ethanol or methanol offers an alternative, it necessitates large volumes of solvent and carries the risk of by-product formation. In contrast, thermal regeneration emerges as a more straightforward and efficient approach, providing the potential to extend catalyst reuse cycles without the need for additional solvent consumption, thus enhancing both practicality and sustainability.

4. Conclusion

Mesoporous silica (MS) was successfully synthesized through soft templating of P123-gelatin via a hydrothermal reaction and calcination at 550°C for 5 hours. TiO_2/MS with a cylindrical morphology of 6 nm and carbon content up to 20% was obtained by using MS as the hard template for tetraethyl orthotitanate infiltration. The crystallinity, surface area, and pore size improved with increasing TiO_2 content in MS. The carbon content in TiO_2/MS also increased with higher TiO_2 due to incomplete decomposition of the Ti precursor organic

groups. The maximum degradation efficiency of methylene blue (MB) by TiO_2/MS was 95%, with 60% from dark adsorption and 35% from the photocatalytic system. The degradation kinetics followed the pseudo-second-order model with a contact time of 120 minutes (30 minutes from dark adsorption and 90 minutes from visible light treatment). The percentage of methylene blue photodegradation with the optimum TiO_2/MS sample after five regeneration cycles was approximately 78%, using the thermal regeneration method at 400°C for 3 hours, resulting in a total efficiency of 495%. This study provides a potential model for reusing catalysts from waste in future applications**.**

Acknowledgements

Authors appreciate funding of International Collaboration Grant 2024 of Sebelas Maret University by Maria Ulfa under contract number 194.2/UN27.22/PT.01.03/2024

References

1. R. Karthik, R. Muthezhilan, A.J. Hussain, K. Ramalingam and V. Rekha, *Effective removal of Methylene Blue dye from water using three different low-cost adsorbents*, Desalin. Water Treat. 57 (2015) 10626–10631.
2. S. Noreen et al., *Iron oxide (Fe2O3) prepared via green route and adsorption efficiency evaluation for an anionic dye : kinetics , isotherms and thermodynamics studies*, J. Mater. Res. Technol. 9 (2020) 4206–4217.
3. J.R. R, A.K. Shukla, K. Kombaiah, J.J. Vijaya and A.M. Tawfeek, *Synthesis, characterization and optical properties of sulfur and fluorine doped ZnO nanostructures for visible light utilized catalysis*, Optik (Stuttg). 148 (2017) 325–331.
4. V. Soltaninejad and A. Maleki, *A green and eco-friendly bionanocomposite film (poly(vinyl alcohol)/TiO_2/chitosan/chlorophyll) by photocatalytic ability, and antibacterial activity under visible-light irradiation*, J. Photochem. Photobiol. A Chem. 404 (2021) 112906.
5. P.R. Ginimuge and S.D. Jyothi, *Methylene Blue : Revisited*, J Anaesth Clin Pharmacol 26 (2010) 517–520.
6. G.L. Dotto, J.M.N. Santos, I.L. Rodrigues, R. Rosa, F.A. Pavan and E.C. Lima, *Adsorption of Methylene Blue by ultrasonic surface modified chitin*, J. Colloid Interface Sci. 446 (2015) 133–140.
7. R. Ata, O. Sacco, V. Vaiano, L. Rizzo, G.Y. Tore and D. Sannino, *Visible light active N-doped TiO_2 immobilized on polystyrene as ef fi cient system for wastewater treatment*, J. Photochem. Photobiol. A Chem. 348 (2017) 255–262.
8. Y. Liu, W. Jin, Y. Zhao, G. Zhang and W. Zhang, *Enhanced catalytic degradation of methylene blue by α-Fe_2O_3/graphene oxide via heterogeneous photo-Fenton reactions*, Appl. Catal. B Environ. 206 (2017) 642–652.
9. P. Chanhom, N. Charoenlap, B. Tomapatanaget and N. Insin, *Colloidal titania-silica-iron oxide nanocomposites and the effect from silica thickness on the photocatalytic and bactericidal activities*, J. Magn. Magn. Mater. 427 (2017) 54–59.
10. M. Ulfa, A. Masykur, A.F. Nofitasari, N.A. Sholeha, S. Suprapto, H. Bahruji et al., *Controlling the Size and Porosity of Sodalite Nanoparticles from Indonesian Kaolin for Pb^{2+} Removal*, Materials (Basel). 15 (2022) 2745.
11. H. Li, V.L. Budarin, J.H. Clark, M. North and X. Wu, *Rapid and efficient adsorption of methylene blue dye from aqueous solution by hierarchically porous, activated starbons ® : Mechanism and porosity dependence*, J. Hazard. Mater. 436 (2022) 129174.
12. J. Gomes, J. Lincho, E. Domingues, R.M. Quinta-Ferreira and R.C. Martins, *N – TiO_2 Photocatalysts : A Review of Their Characteristics and Capacity for Emerging Contaminants Removal*, Water 11 (2019) 373.
13. A. Kamel, H. Al, J. Wu and S.R. Upreti, *Continuous ozonation of methylene blue in water*, J. Water Process Eng. 8 (2015) 142–150.
14. S. Rajagopal, B. Paramasivam and K. Muniyasamy, *Separation and Puri fi cation Technology Photocatalytic removal of cationic and anionic dyes in the textile wastewater by H_2O_2 assisted TiO_2 and micro-cellulose composites*, Sep. Purif. Technol. 252 (2020) 117444.
15. D. Cani, J.C. Van Der Waal and P.P. Pescarmona, *Highly-accessible, doped TiO_2 nanoparticles embedded at the surface of SiO_2 as photocatalysts for the degradation of pollutants under visible and UV radiation*, Appl. Catal. A, Gen. 621 (2021) 118179.
16. M. Khairy and W. Zakaria, *Effect of metal-doping of TiO_2 nanoparticles on their photocatalytic activities toward removal of organic dyes*, Egypt. J. Pet. 23 (2014) 419–426.
17. M. Barczak, R. Dobrowolski, P. Borowski and D.A. Giannakoudakis, *Pyridine- , thiol- and amine-functionalized mesoporous silicas for adsorptive removal of pharmaceuticals*, Microporous Mesoporous Mater. 299 (2020) 110132.
18. Y. Hu, J. Wang, Z. Zhi, T. Jiang and S. Wang, *Facile synthesis of 3D cubic mesoporous silica microspheres with a controllable pore size and their application for improved delivery of a water-insoluble drug*, J. Colloid Interface Sci. 363 (2011) 410–417.
19. M. Ulfa, D. Prasetyoko, A.H. Mahadi and H. Bahruji, *Size tunable mesoporous carbon microspheres using Pluronic F127 and gelatin as co-template for removal of ibuprofen*, Sci. Total Environ. 711 (2020) 135066.
20. M. Ulfa, D. Prasetyoko, H. Bahruji and R.E. Nugraha, *Green Synthesis of Hexagonal Hematite (α-Fe_2O_3) Flakes Using Pluronic F127-Gelatin Template for Adsorption and Photodegradation of Ibuprofen*, Materials (Basel). 14 (2021) 6779.
21. U. Balachandran and N.G. Eror, *Raman Spectra of Titanium Dioxide*, J. Solid State Chem. 42 (1982) 276–282.
22. J.H. Roque-Ruiz, H. Martínez-Máynez, M.A. Zalapa-Garibay, A. Arizmendi-Moraquecho, R. Farias and S.Y. Reyes-López, *Surface enhanced Raman spectroscopy in nanofibers mats of SiO2-TiO2-Ag*, Results Phys. 7 (2017) 2520–2527.
23. I. Fatimah, N. Iman, I. Sahroni and M.M. Musawwa, *Physicochemical characteristics and photocatalytic performance of TiO_2/SiO_2 catalyst synthesized using biogenic silica from bamboo leaves*, Heliyon 5 (2019) e02766.
24. *Simultaneous tartrazine-tetracycline removal and hydrogen production in the hybrid electrocoagulation-photocatalytic process using g-C3N4/TiNTAs*. Commun. Sci. Technol. 9 (2024) 46-56.
25. *Utilizing Pometia Pinnata leaf extract in microwave synthesis of ZnO nanoparticles: Investigation into photocatalytic properties*. Commun. Sci. Technol. 9 (2024) 94-99.